

1   **Optimization of an LNP-mRNA vaccine candidate targeting SARS-CoV-2**  
2   **receptor-binding domain**

3

4   Kouji Kobiyama<sup>1,7</sup>, Masaki Imai<sup>2,7</sup>, Nao Jounai<sup>3,7</sup>, Misako Nakayama<sup>4,7</sup>, Kou Hioki<sup>1</sup>,  
5   Kiyoko Iwatsuki-Horimoto<sup>2</sup>, Seiya Yamayoshi<sup>2</sup>, Jun Tsuchida<sup>1</sup>, Takako Niwa<sup>5</sup>, Takashi  
6   Suzuki<sup>5</sup>, Mutsumi Ito<sup>2</sup>, Shinya Yamada<sup>2</sup>, Tokiko Watanabe<sup>2</sup>, Maki Kiso<sup>2</sup>, Hideo  
7   Negishi<sup>1</sup>, Burcu Temizoz<sup>1</sup>, Hirohito Ishigaki<sup>4</sup>, Yoshinori Kitagawa<sup>6</sup>, Cong Thanh  
8   Nguyen<sup>4</sup>, Yasushi Itoh<sup>4,8</sup>, Fumihiko Takeshita<sup>3,8</sup>, Yoshihiro Kawaoka<sup>2,8</sup>, and Ken J.  
9   Ishii<sup>1,8</sup>

10

11   <sup>1</sup>Division of Vaccine Science,

12   <sup>2</sup>Division of Virology, Department of Microbiology and Immunology, The Institute of  
13   Medical Science, The University of Tokyo, 4-6-1 Shirokanedai, Minato-ku, Tokyo  
14   108-8639, Japan.

15   <sup>3</sup>Biologics Division, Vaccine Research Laboratories, Daichi Sankyo Co., Ltd. 1-16-13,  
16   Kitakasai, Edogawa-ku, Tokyo 134-0081, Japan

17   <sup>4</sup>Division of Pathogenesis and Disease Regulation, Department of Pathology, Shiga  
18   University of Medical Science, Setatsukinowa, Otsu, Shiga 520-2192, Japan

19   <sup>5</sup>Biologics Division, Modality Research Laboratories, Daichi Sankyo Co., Ltd. 1-2-58,  
20   Hiromachi, Shinagawa-ku, Tokyo 134-0081, Japan

21   <sup>6</sup>Division of Microbiology and Infectious Diseases, Department of Pathology, Shiga  
22   University of Medical Science, Setatsukinowa, Otsu, Shiga 520-2192, Japan

23

24   <sup>7</sup>The authors are contributed to this work equally

25

26   <sup>8</sup>Correspondence should be addressed to

27   Ken J. Ishii [kenishii@ims.u-tokyo.ac.jp](mailto:kenishii@ims.u-tokyo.ac.jp), or

28   Yoshihiro Kawaoka [kawaoka@ims.u-tokyo.ac.jp](mailto:kawaoka@ims.u-tokyo.ac.jp)

29   Fumihiko Takeshita [takeshita.fumihiko.aw@daiichisankyo.co.jp](mailto:takeshita.fumihiko.aw@daiichisankyo.co.jp)

30   Yasushi Itoh [yasushii@belle.shiga-med.ac.jp](mailto:yasushii@belle.shiga-med.ac.jp)

31

32

33           **In 2020, two mRNA-based vaccines, encoding the full length of severe**  
34           **acute respiratory syndrome coronavirus 2 (SARS-CoV-2) spike protein, have been**  
35           **introduced for control of the coronavirus disease (COVID-19) pandemic<sup>1,2</sup>.**  
36           **However, reactogenicity, such as fever, caused by innate immune responses to the**  
37           **vaccine formulation remains to be improved. Here, we optimized a lipid**  
38           **nanoparticle (LNP)-based mRNA vaccine candidate, encoding the SARS-CoV-2**  
39           **spike protein receptor-binding domain (LNP-mRNA-RBD), which showed**  
40           **improved immunogenicity by removing reactogenic materials from the vaccine**  
41           **formulation and protective potential against SARS-CoV-2 infection in cynomolgus**  
42           **macaques. LNP-mRNA-RBD induced robust antigen-specific B cells and follicular**  
43           **helper T cells in the BALB/c strain but not in the C57BL/6 strain; the two strains**  
44           **have contrasting abilities to induce type I interferon production by dendritic cells.**  
45           **Removal of reactogenic materials from original synthesized mRNA by HPLC**  
46           **reduced type I interferon (IFN) production by dendritic cells, which improved**  
47           **immunogenicity. Immunization of cynomolgus macaques with an LNP**  
48           **encapsulating HPLC-purified mRNA induced robust anti-RBD IgG in the plasma**  
49           **and in various mucosal areas, including airways, thereby conferring protection**  
50           **against SARS-CoV-2 infection. Therefore, fine-tuning the balance between the**  
51           **immunogenic and reactogenic activity of mRNA-based vaccine formulations may**  
52           **offer safer and more efficacious outcomes.**

53           The SARS-CoV-2 spike glycoprotein contains a receptor-binding domain  
54           (RBD) that binds to human angiotensin-converting enzyme 2 (hACE2) as a receptor to  
55           facilitate membrane fusion and cell entry<sup>3</sup>. Recent evidence suggests that the immune  
56           response to the SARS-CoV-2 spike protein is the key to controlling SARS-CoV-2  
57           infection; a vaccine that can induce robust and specific T and B cells against the  
58           receptor-binding domain (RBD) of the spike protein antigen of SARS-CoV-2 may be  
59           ideal for protective efficacy and safety<sup>4</sup>. Accordingly, various animal experiments have  
60           demonstrated that the induction of humoral and cellular immune responses to the RBD  
61           by various types of vaccines confers protective efficacy with no signs of detrimental  
62           outcomes such as antibody-dependent enhancement<sup>5,6</sup>.

63           Concurrently with animal studies, a number of human clinical trials with  
64           various types of vaccines against COVID-19 have been initiated, conducted, and  
65           completed globally within a year after the viral genome sequence was reported in

66 Wuhan, China, in December 2019<sup>7</sup>. Two mRNA vaccines encoding the full-length spike  
67 protein of SARS-CoV-2 have undergone Phase I-II-III trials, which were completed in  
68 nine months and approved by regulatory authorities in various countries as well as the  
69 WHO<sup>1,2,8-10</sup>. The results of their initial phase I-II clinical trials suggest that in both  
70 younger and older adults, the two vaccine candidates elicited similar dose-dependent  
71 SARS-CoV-2–neutralizing geometric mean titers, which were equivalent to that of a  
72 panel of SARS-CoV-2 convalescent serum samples<sup>9,10</sup>. It is worth noting that an mRNA  
73 vaccine (BNT162b2) encoding the full length of the SARS-CoV-2 spike protein was  
74 associated with a lower incidence and severity of systemic reactions than another  
75 mRNA vaccine encoding the RBD of spike protein (BNT162b1), particularly in older  
76 adults<sup>10</sup>. A few scientific explanations have been offered: one is the amount of mRNA in  
77 the RBD-mRNA vaccine, whose molar ratio is five times more than that of the  
78 full-length mRNA vaccine due to an RNA length shorter by 1/5 at the same dose.  
79 Although each RNA modification in the *in vitro* translated (IVT) mRNA to avoid innate  
80 immune recognition was made, the number or position of the modified nucleoside of the  
81 mRNAs may alter their immunostimulatory activity, acting as an endogenous adjuvant.  
82 Here, we optimized an mRNA vaccine candidate encoding SARS-CoV-2 spike protein  
83 RBD (319–541 aa) encapsulated in lipid nanoparticles (LNP-mRNA-RBD).

84 To date, a mouse model using the BALB/c strain has been commonly  
85 used<sup>6,11,12</sup>, except for one study where C57BL/6 mice were immunized with  
86 LNP-mRNA encoding SARS-CoV-2 RBD, resulting in antigen-specific germinal center  
87 (GC) B cells and follicular helper CD4<sup>+</sup> T cells (T<sub>FH</sub>) cells<sup>13</sup>.

88 First, we immunized 6–8-week-old female mice of either the C57BL/6 or  
89 BALB/c strains intramuscularly with 3 µg of LNP-mRNA-RBD on days 0 and 14.  
90 Unexpectedly, after two intramuscular immunizations, LNP-mRNA-RBD induced  
91 significantly higher anti-RBD antibody responses in BALB/c mice but not in C57BL/6  
92 mice in this study (**Fig. 1a, Extended Fig 1**). To understand why LNP-mRNA-RBD  
93 immunogenicity for antigen-specific B cell responses was different among mouse  
94 strains, we further examined whether LNP-mRNA-RBD induces T<sub>FH</sub> and GC B cells  
95 collected from the draining popliteal lymph nodes (pLN) and analyzed by flow  
96 cytometry (**Extended data Fig. 2**). In correlation with serum antibody responses, the  
97 frequency (%) of both T<sub>FH</sub> (CD4<sup>+</sup>CD185<sup>+</sup>PD-1<sup>+</sup> cells) and GC B cells  
98 (CD38<sup>+</sup>GL7<sup>+</sup>CD19<sup>+</sup> cells) in the immunized pLN was significantly higher in BALB/c

99 mice than that in C57BL/6 mice (**Fig. 1b-e**) after LNP-mRNA-RBD immunization.

100 To further evaluate antigen-specific CD8<sup>+</sup> and other CD4<sup>+</sup> T cells induced by  
101 LNP-mRNA-RBD, we synthesized 128 peptides, consisting of a 20-aa sequence of  
102 spike protein with 10 overlapping aa divided into eight pools containing 16 peptides in  
103 one pool (**Fig. 1f**). After two LNP-mRNA-RBD immunizations in either mouse strain,  
104 *in vitro* re-stimulation of the immunized spleen with peptide pools 3 and 4 induced  
105 substantial IFN- $\gamma$  production in C57BL/6 mice, while in BALB/c mice this was  
106 achieved with peptide pool 3 (**Fig. 1g and h, Extended data Fig. 3a and b**). IL-13  
107 production was not found in the supernatant of the spleen cell culture with peptides in  
108 either C57BL/6 or BALB/c mice (**Extended data Fig. 3c and d**). To further  
109 characterize LNP-mRNA-RBD-induced T cells, we performed intracellular cytokine  
110 staining of three antigen-specific type-1 cytokines (IL-2, IFN- $\gamma$ , and TNF- $\alpha$ ) produced  
111 by the immunized spleen T cells re-stimulated with peptide pools 2, 3, or 4. Spike  
112 antigen-specific polyfunctional CD8<sup>+</sup> and CD4<sup>+</sup> T cells were significantly upregulated  
113 in LNP-mRNA-RBD-immunized BALB/c mice after re-stimulating the spleen cells  
114 with peptide pools 3 and 4 (**Fig. 1h, Extended data Fig. 4b and 5b**). However, those in  
115 the immunized C57BL/6 mice showed substantial polyfunctional CD8<sup>+</sup> T cells and  
116 weak CD4<sup>+</sup> T cell responses (**Fig. 1g, Extended data Fig. 4a and 5a**). These data  
117 clearly demonstrate that LNP-mRNA-RBD induces robust B and T cell responses in  
118 BALB/c mice but relatively weak T cell and B cell responses in C57BL/6 mice,  
119 suggesting the immunogenic profile of LNP-mRNA-RBD is different between these  
120 mouse strains.

121 Nucleic acid-based vaccines are known to utilize their backbone DNA or  
122 RNA as built-in adjuvants<sup>14-16</sup>. In LNP-mRNA vaccines, it has been shown that mRNA  
123 itself acts as an endogenous adjuvant sensed by Toll-like receptors 3, 7, or 8 and/or  
124 cytosolic RNA sensors such as RIG-I and MDA5<sup>17</sup>. Kariko et al. reported that  
125 modification of RNA by methylation or incorporating modified nucleoside such as  
126 pseudouridine enables the escape from innate immune sensing, thereby improving  
127 translation efficiency<sup>18,19</sup>. Several studies have revealed that type I IFN interferes with  
128 the CD8 T cell responses elicited by LNP-mRNA and the translation efficiency of the  
129 encoded protein<sup>20,21,22</sup>. In addition to T cell responses, BNT162b1 showed higher  
130 reactogenicity than BNT162b2 in the clinical trial; therefore, BNT162b2 has been  
131 selected for further development in a Phase III clinical trial<sup>10</sup>. The reason for the

132 difference in reactogenicity remains unclear, but the authors considered that  
133 immunostimulatory activity of the mRNA in LNP formulation might be attributed to its  
134 reactogenicity<sup>10</sup>.

135 In order to translate our findings from mice to humans, we then examined  
136 whether LNP-mRNA-RBD triggers type I IFN production from human PBMCs. When  
137 mixed with LNP-mRNA-RBD *in vitro*, PBMCs from three healthy humans produced a  
138 higher amount of IFN- $\alpha$  than that induced by LNP-mRNA-Full (**Fig. 2a**). We then  
139 performed a similar experiment using mouse bone marrow-derived dendritic cells  
140 (BM-DCs) from either C57BL/6 or BALB/c mice. Surprisingly, a high level of IFN- $\alpha$   
141 was observed upon culture with LNP-mRNA-full or LNP-mRNA-RBD in C57BL/6  
142 mice, but very low or no IFN- $\alpha$  production was observed in BALB/c mice (**Fig. 2b**).  
143 LNP-mRNA products usually contain undesirable RNA, such as dsRNA as TLR3  
144 ligand<sup>22</sup>, produced during the manufacturing process, which might affect innate immune  
145 activation. To remove such RNA byproducts, we performed HPLC purification (**data**  
146 **not shown**) and then the resultant mRNA containing the active ingredient was  
147 encapsulated in LNP [RBD (HPLC)]. RBD (HPLC) showed significantly less potential  
148 in production of type I IFN from both human PBMCs and GM-DCs (**Fig. 2a and b**). In  
149 order to examine the immunogenicity, C57BL/6 or BALB/c mice were administered  
150 with RBD (HPLC) or LNP-mRNA-RBD. Of interest, RBD (HPLC) showed  
151 significantly higher levels of the RBD-specific B cell response than LNP-mRNA-RBD,  
152 including serum IgG1, IgG2, and total IgG in both BALB/c and C57BL/6 mice (**Fig. 2c**  
153 **and Extended Fig. 6a**). In particular, RBD (HPLC) induced significantly higher  
154 number of GC B cells in the draining lymph nodes of the C57BL/6 mice than  
155 LNP-mRNA-RBD (**Fig. 2d and e**). In addition to antibody responses, effects of  
156 RNA-purification on antigen-specific T cell responses were further examined. RBD  
157 (HPLC) induced higher frequency of the RBD-specific polyfunctional CD8 $^{+}$  and CD4 $^{+}$   
158 T cells that produced significantly more IFN- $\gamma$  and other type-1 cytokines, but not  
159 type-2 cytokines such as IL-13, in response to peptide pools 3 or 4 re-stimulation than  
160 LNP-mRNA-RBD (**Fig. 2f-i, and Extended Fig. 6b-e, 7, 8**).

161 To further translate these findings to a more relevant pre-clinical evaluation of  
162 RBD (HPLC), non-human primates (NHPs), cynomolgus macaques, were chosen for  
163 further study. In this study, we immunized four macaques intramuscularly with RBD  
164 (HPLC) with two macaques as mock controls. After the first immunization, RBD

165 (HPLC) induced an anti-RBD-specific antibody, and the second immunization enhanced  
166 these responses (**Fig. 3b**). Neutralizing antibodies were also induced by RBD (HPLC)  
167 vaccination (**Fig. 3c**). We further examined antigen-specific antibody responses in swab  
168 samples. Interestingly, following intramuscular immunization, levels of RBD-specific  
169 IgG in the swab samples from conjunctiva, nasal cavity, oral cavity, trachea, and rectum  
170 were significantly higher in RBD (HPLC) group than in the mock group (**Fig. 3d**).

171 Individual macaques administered with RBD (HPLC) showed drastically  
172 lower RNA levels of SARS-CoV-2 (**Fig. 4a**) and infectious virus (**Fig. 4b**) in the swab  
173 at day 1 post-infection than those administered with mock. Viral RNA levels in the  
174 trachea, bronchus, and lung were lower in vaccinated macaques at day 7 (**Fig. 4c and**  
175 **Extended Fig. 9**). All mock-administered macaques manifested fever and pneumonia  
176 after viral infection, which were not observed in immunized macaques (**Extended Fig.**  
177 **10 and 11**). These results suggest that RBD (HPLC) administration confers protection  
178 against SARS-CoV-2 infection. Histological analysis of the lung at 7 days post  
179 infection demonstrated infiltration of lymphocytes and neutrophils, alveolar wall  
180 thickening, and viral protein in macaques administered with mock but not in those  
181 administered with RBD (HPLC) (**Fig. 4d and 4e**). Accordingly, histological scores of  
182 the lung in macaques administered with RBD (HPLC) were lower than those  
183 administered with mock (**Fig. 4f**). Of importance, intramuscular administration with  
184 RBD (HPLC) induced the development of bronchus-associated lymphoid tissue (BALT)  
185 (**Fig. 4d**), although intramuscular immunization induced RBD-specific IgG, but not IgA,  
186 in swab samples without intranasal and intratracheal virus challenge (**Fig. 3b**).  
187 Interestingly, the IgG titer was slightly reduced or similar after viral challenge (**Fig. 3d**).  
188 These results suggest that the induced antibody in the mucosa through BALT formation,  
189 such as the nasal and trachea mucosa, might capture and neutralize SARS-CoV-2,  
190 resulting in the reduction of viral RNA and infective virus in the swab at day 1  
191 post-challenge.

192 In this study, we evaluated the nonclinical efficacy of LNP-mRNA vaccine  
193 candidates targeting SARS-CoV-2 RBD. First, LNP-mRNA-RBD showed higher  
194 immunogenicity only in BALB/c mice than in C57BL/6 mice (**Fig. 1a**). We initially  
195 interpreted the data by suggesting the less T cell epitopes of the RBD in C57/BL6 as the  
196 cause. In fact, CD4 Tfh induction was lower in C57BL/6 mice than that of BALB/c  
197 mice even after HPLC purification (**Fig. 1e and 2e**). However, recent clinical trials by

198 BioNTech/Pfizer showed that an mRNA vaccine that encoded the RBD resulted in a  
199 high titer of RBD-specific IgG and neutralizing antibodies in humans and monkeys.  
200 These results suggest that RBD does contain T cell epitopes, at least in primates<sup>6,10</sup>.  
201 These data led us to hypothesize that the difference in vaccine-induced adaptive  
202 immune responses is altered by the species- or strain-specific innate immune responses  
203 to the LNP-mRNA formulation, which is shown to interfere with the mRNA expression  
204 of the protein antigen of interest, thereby reducing immunogenicity and efficacy<sup>16</sup>. Our  
205 data strongly suggest that optimization of purification and formulation of LNP-mRNA  
206 contributes to improvement of LNP-mRNA immunogenicity with less reactogenicity.

207 It is of note that macaques administered with LNP-mRNA targeting RBD  
208 acquired significantly high levels of protective IgG specific to SARS-CoV-2 in mucosal  
209 swab samples from conjunctiva, oral cavity, nasal cavity, trachea, bronchus, and rectum  
210 (Fig. 3d and data not shown). Corbett KS et al. recently demonstrated that vaccination  
211 of NHPs with LNP-mRNA encoding the full-length spike antigen (mRNA-1273)  
212 induced robust SARS-CoV-2 neutralizing activity and rapid protection in the upper and  
213 lower airways and showed that the IgG level in the BALF was higher than the IgA level  
214 after the infection, although whether the vaccine antigen-specific IgG was induced  
215 before the virus challenge was not shown<sup>23</sup>. Although HPLC-purified  
216 LNP-mRNA-RBD elicited RBD-specific mucosal IgG, no RBD-specific IgA was  
217 detected (data not shown), indicating that the mucosal IgG through BALT formation or  
218 leaked from the blood circulation, which may be critical for the protective efficacy of  
219 LNP-mRNA-RBD. Further detailed analyses are needed to clarify whether LNP-mRNA  
220 induces unique and/or specific immune responses including IgG secretion in the mucosa  
221 after intramuscular vaccination.

222 Based on our results obtained in murine and NHP models, reduction of  
223 reactogenicity without losing immunogenicity, in other words, fine-tuning of the  
224 balance between endogenous adjuvant activity and antigen translation efficiency of  
225 LNP-mRNA, may provide a means towards better efficacy and safety and will also be  
226 crucial for the development of anti-SARS-CoV2 vaccines in the near future.  
227

228 **Figure legends**

229 **Figure 1. Mouse strain-specific immunogenicity of mRNA vaccine against**  
230 **SARS-CoV-2 RBD.**

231 **(a–e, g, and h)** Six to eight week-old C57BL/6 and BALB/c mice were  
232 intramuscularly immunized with mock or LNP-mRNA-RBD (3  $\mu$ g) at days 0 and 14.  
233 **(a)** Two weeks after the second immunization, plasma anti-RBD antibody titers were  
234 measured using ELISA. **(b–e)** Popliteal lymph nodes were collected from immunized  
235 mice. **(b–d)** GC B cells were gated as GL7 $^{+}$ CD38 $^{-}$ CD19 $^{+}$  cells. **(e)** T<sub>FH</sub> cells were gated  
236 as CD185 $^{+}$ PD-1 $^{+}$ CD3 $\epsilon$  $^{+}$ CD4 $^{+}$  T cells. **(f)** Overlapping peptides of SARS-CoV-2 spike  
237 protein. Overlapping peptides were divided into eight pools, and each pool contained 16  
238 peptides. **(g–h)** Cells were harvested from the spleen of mRNA-RBD immunized mice  
239 and re-stimulated with pooled peptides for 24 h. IFN- $\gamma$  levels in the culture supernatant  
240 were measured using ELISA. **(g–h)** Percentages of cytokine-producing CD8 $^{+}$  and CD4 $^{+}$   
241 T cells after stimulation with pools 2, 3, and 4 for 6 h with protein transport inhibitor are  
242 shown in a pie chart. 3 $^{+}$ : IFN- $\gamma$  $^{+}$ IL-2 $^{+}$ TNF- $\alpha$  $^{+}$ , 2 $^{+}$ : IFN- $\gamma$  $^{+}$ IL-2 $^{+}$ , IFN- $\gamma$  $^{+}$ TNF- $\alpha$  $^{+}$ , and  
243 IL-2 $^{+}$ TNF- $\alpha$  $^{+}$ , 1 $^{+}$ : IFN- $\gamma$  $^{+}$ , IL-2 $^{+}$ , and TNF- $\alpha$  $^{+}$ .  $N = 4–5$  mice per group, mean  $\pm$  SEM, \* $p$   
244  $< 0.05$  by Mann-Whitney test.

245

246 **Figure 2. HPLC purification improves the immunogenicity of mRNA vaccine. (a)**  
247 Human PBMCs from non-infected individuals were stimulated with LNP-mRNA-Full  
248 (0.4, 2, and 10  $\mu$ g/mL), LNP-mRNA-RBD (0.4, 2, and 10  $\mu$ g/mL), or  
249 LNP-mRNA-RBD (HPLC) (0.4, 2, and 10  $\mu$ g/mL) for 24 h. IFN- $\alpha$  level in the culture  
250 supernatant was measured using ELISA. **(b)** Bone-marrow-derived dendritic cells  
251 (BM-DCs) from C57BL/6 and BALB/c mice were stimulated by LNP-mRNA-Full (0.4,  
252 2, and 10  $\mu$ g/mL), LNP-mRNA-RBD (0.4, 2, and 10  $\mu$ g/mL), or LNP-mRNA-RBD  
253 (HPLC) (0.4, 2, and 10  $\mu$ g/mL) for 24 h. IFN- $\alpha$  level in the culture supernatant was  
254 measured using ELISA. **(c–i)** C57BL/6 mice were intramuscularly immunized with  
255 mock, LNP-mRNA-RBD (3  $\mu$ g), or LNP-mRNA-RBD (HPLC) (3  $\mu$ g) at days 0 and 14.  
256 **(c)** Two weeks after the second immunization, plasma anti-RBD antibody titers were  
257 measured using ELISA. **(d and e)** Popliteal lymph nodes were collected from  
258 immunized mice. **(d)** GC B cells were gated as GL7 $^{+}$ CD38 $^{-}$ CD19 $^{+}$  cells. **(e)** T<sub>FH</sub> cells  
259 were gated as CD185 $^{+}$ PD-1 $^{+}$ CD3 $\epsilon$  $^{+}$ CD4 $^{+}$  T cells. **(f and g)** Cells were harvested from  
260 the spleen of immunized mice and re-stimulated with pooled peptides for 24 h. IFN- $\gamma$

261 level in the culture supernatant was measured using ELISA. Percentages of  
262 cytokine-producing CD8<sup>+</sup> and CD4<sup>+</sup> T cells after stimulation of peptide pools 3 and 4  
263 for 6 h with protein transport inhibitors are shown in a pie chart. 3<sup>+</sup>: IFN- $\gamma$ <sup>+</sup>IL-2<sup>+</sup>TNF- $\alpha$ <sup>+</sup>,  
264 2<sup>+</sup>: IFN- $\gamma$ <sup>+</sup>IL-2<sup>+</sup>, IFN- $\gamma$ <sup>+</sup>TNF- $\alpha$ <sup>+</sup>, and IL-2<sup>+</sup>TNF- $\alpha$ <sup>+</sup>, 1<sup>+</sup>: IFN- $\gamma$ <sup>+</sup>, IL-2<sup>+</sup>, and TNF- $\alpha$ <sup>+</sup>. (h  
265 and i) Representative data from Figure 2f, g, Extended data Fig. 8, and 9 are shown.  
266 IFN- $\gamma$ <sup>+</sup>IL-2<sup>+</sup>TNF- $\alpha$ <sup>+</sup> and IFN- $\gamma$ <sup>+</sup>TNF- $\alpha$ <sup>+</sup> CD8<sup>+</sup> T cell are shown as a scatter dot plot.  $N =$   
267 4–5 mice per group, mean  $\pm$  SEM, \*  $p < 0.05$  by ANOVA followed by Dunn's multiple  
268 comparisons test.

269

270 **Figure 3. HPLC-purified LNP-mRNA-RBD induces RBD-specific antibodies in the**  
271 **plasma and swab samples of non-human primates** (a) Schedule of immunization,  
272 infection, and sample collection. (b–c) Cynomolgus macaques were intramuscularly  
273 immunized with mock or LNP-mRNA-RBD (HPLC) (100  $\mu$ g) at days 0 and 21. (b)  
274 Plasma anti-RBD antibody titer at days 0, 7, 14, 21, 28, and 7 dpi were measured using  
275 ELISA. (c) Neutralizing activity against SARS-CoV-2 infection were measured by  
276 neutralization assay. (d) Anti-RBD IgG titers in the swab samples (conjunctiva, oral  
277 cavity, nasal cavity, tracheal, and rectum) were measured using ELISA. Black arrows  
278 indicate date of vaccination, and red arrows indicate infection date.

279

280 **Figure 4. HPLC-purified LNP-mRNA-RBD protects against SARS-CoV-2**  
281 **infection in non-human primates.** One week after the second immunization,  
282 SARS-CoV-2 ( $2 \times 10^7$  PFU) was inoculated into conjunctiva, nasal cavity, oral cavity,  
283 and trachea of cynomolgus. (a) Viral RNA and (b) viral titers in the swab sample were  
284 measured by RT-PCR and a cell culture method. (c) Viral RNA in the lung tissues were  
285 measured by RT-PCR. RU: right upper lobe, RM: right middle lobe, RL: right lower  
286 lobe, LU: left upper lobe, LM: left middle lobe, LL: left lower lobe. (d) HE staining and  
287 (e) immunohistochemical staining of viral nucleocapsid protein in lung sections from  
288 Mock (left) and mRNA-RBD (HPLC) (right) immunized macaques. (f) The average  
289 histological scores of eight sections in each macaque were evaluated in a blinded  
290 manner.

291

292

293

294 **Extended data Fig 1. LNP-mRNA-RBD vaccine induces ectodomain-specific**  
295 **antibody responses in BALB/c mice.** C57BL/6 and BALB/c mice were  
296 intramuscularly immunized with mock or LNP-mRNA-RBD (3  $\mu$ g) on days 0 and 14.  
297 Two weeks after the second immunization, plasma anti-ECD antibody titers were  
298 measured using ELISA.  $N = 4-5$  mice per group, mean  $\pm$  SEM,  $*p < 0.05$  by  
299 Mann-Whitney test.

300

301 **Extended data Fig 2. Gating strategy for GC B and T<sub>FH</sub> cells.** Cells were harvested  
302 from popliteal lymph nodes of immunized mice and stained for GC B and T<sub>FH</sub> cells.  
303 Cells were gated for lymphocyte size, singlets, live, T or B cells, and T<sub>FH</sub> or GC B cells.

304

305 **Extended data Fig 3. T cell responses to LNP-mRNA-RBD.** Cells were harvested  
306 from the spleen of mRNA-immunized mice, re-stimulated by the spike protein peptide  
307 pool, ECD, or RBD for 24 h. IFN- $\gamma$  and IL-13 levels in the culture supernatant were  
308 measured using ELISA.  $N = 4-5$  mice per group, mean  $\pm$  SEM,  $*p < 0.05$  by ANOVA  
309 followed by Sidak's multiple comparisons test.

310

311 **Extended data Fig 4. CD8 T cell responses to the mRNA vaccine.** Cells were  
312 harvested from the spleen of immunized mice and re-stimulated by pooled peptides for  
313 6 h with a protein transport inhibitor. The percentage of cytokine-producing CD8 $^{+}$  T  
314 cells was analyzed by flow cytometry.  $N = 4-5$  mice per group, mean  $\pm$  SEM,  $*p < 0.05$   
315 by Mann-Whitney test.

316

317 **Extended data Fig 5. CD4 T cell responses to the mRNA vaccine.** Cells were  
318 harvested from the spleen of immunized mice and re-stimulated by pooled peptides for  
319 6 h with a protein transport inhibitor. Percentage of cytokine-producing CD4 $^{+}$  T cells  
320 was analyzed by flow cytometry.  $N = 4-5$  mice per group, mean  $\pm$  SEM,  $*p < 0.05$  by  
321 Mann-Whitney test.

322

323 **Extended data Fig 6. T cell responses to an HPLC-purified mRNA vaccine in**  
324 **C57/BL6 mice. (a)** C57/BL6 and BALB/c mice were intramuscularly immunized with  
325 mock, mRNA-RBD, or RBD (HPLC) (3  $\mu$ g) on days 0 and 14. Two weeks after the  
326 second immunization, serum anti-ECD antibody titers were measured using ELISA. **(b-**

327 e) Cells were harvested from the spleen of mRNA-immunized mice, re-stimulated by  
328 the peptide pool of spike protein, ECD, or RBD for 24 h. IFN- $\gamma$  and IL-13 levels in the  
329 culture supernatant were measured using ELISA.  $N = 4$  mice per group, mean  $\pm$  SEM, \*  
330  $p < 0.05$  by ANOVA followed by Dunn's or Sidak's multiple comparisons test.

331

332 **Extended data Fig 7. T cell responses to an HPLC-purified mRNA vaccine in**  
333 **C57/BL6 mice.** Cells were harvested from the spleen of immunized mice and  
334 re-stimulated by pooled peptides for 6 h with a protein transport inhibitor. The  
335 percentage of cytokine-producing CD8 $^{+}$  and CD4 $^{+}$  T cells was analyzed by flow  
336 cytometry.  $N = 4$  mice per group, mean  $\pm$  SEM, \*  $p < 0.05$  by ANOVA followed by  
337 Dunn's multiple comparisons test.

338

339 **Extended data Fig 8. T cell responses to an HPLC-purified mRNA vaccine in**  
340 **BALB/c mice.** Cells were harvested from the spleen of immunized mice and  
341 re-stimulated with pooled peptides for 6 h with a protein transport inhibitor. The  
342 percentage of cytokine-producing CD8 $^{+}$  and CD4 $^{+}$  T cells was analyzed by flow  
343 cytometry.  $N = 4$  mice per group, mean  $\pm$  SEM, \*  $p < 0.05$  by ANOVA followed by  
344 Dunn's multiple comparisons test.

345

346 **Extended data Fig 9. HPLC-purified mRNA vaccine protects against SARS-CoV-2**  
347 **infection in non-human primates.** One week after the second immunization,  
348 SARS-CoV-2 ( $2 \times 10^7$  PFU) was inoculated into conjunctiva, nasal cavity, oral cavity,  
349 and trachea of cynomolgus. Viral RNA in the trachea and bronchus tissues were  
350 measured by RT-PCR.

351

352 **Extended data Fig 10. Change in body temperature after SARS-CoV-2 infection**  
353 One week after the second immunization, SARS-CoV-2 ( $2 \times 10^7$  PFU) was inoculated  
354 into conjunctiva, nasal cavity, oral cavity, and trachea of cynomolgus. Body temperature  
355 was recorded from two days before infection using telemetry transmitters and a  
356 computer.

357

358 **Extended data Fig 11. The HPLC-purified mRNA vaccine protects against**  
359 **SARS-CoV-2-induced pneumonia.** X-ray radiographs of macaques were taken before

360 and after SARS-CoV-2 infection.

361

362

363 **Material and Methods**

364

365 **Mice**

366 Six to eight week-old C57BL/6 and BALB/c mice were purchased from CLEA, Japan.  
367 The mice were maintained under specific pathogen-free conditions. All mouse studies  
368 were approved by the Animal Experiment Committee of the Institute of Medical  
369 Science, University of Tokyo.

370

371 **Cynomolgus macaque**

372 Seven to ten-year-old female cynomolgus macaques born at Shiga University of  
373 Medical Science and originating from Philippines, Vietnam, and China were used. All  
374 procedures were performed under ketamine and xylazine anesthesia, and all efforts were  
375 made to minimize suffering. Food pellets of CMK-2 (CLEA Japan, Inc., Tokyo, Japan)  
376 were provided once a day after recovery from anesthesia and drinking water was  
377 available *ad libitum*. The animals were singly housed in cages under controlled  
378 conditions of light (12-h light/12-h dark cycle, lights on at 8:00 a.m.). The macaques  
379 were challenged with the SARS-CoV-2 ( $2 \times 10^7$  PFU/7 mL HBSS), which was  
380 inoculated into the conjunctiva (0.05 mL  $\times$  2), nostrils (0.5 mL  $\times$  2), oral cavity (0.9  
381 mL), and trachea (5 mL) with pipettes and catheters under ketamine/xylazine anesthesia.  
382 Under ketamine/xylazine anesthesia, two cotton sticks (Eiken Chemical, Ltd., Tokyo,  
383 Japan) were used to collect fluid samples from the conjunctivas, nasal cavities, oral  
384 cavities and tracheas, and the sticks were subsequently immersed in 1 mL of Dulbecco's  
385 modified Eagle medium (DMEM, Nacalai Tesque, Kyoto, Japan) containing 0.1%  
386 bovine serum albumin (BSA) and antibiotics. A bronchoscope (MEV-2560; Machida  
387 Endoscope Co. Ltd., Tokyo, Japan) and cytology brushes (BC-203D-2006; Olympus  
388 Co., Tokyo, Japan) were used to obtain bronchial samples.

389

390 **LNP-mRNA vaccines**

391 T7 RNA polymerase-mediated transcription *in vitro* was used to synthesize the mRNA  
392 from a linearized DNA template, which flanked the open-reading frames of RBD with  
393 the 5' and 3' untranslated regions and a poly-A tail. Messenger RNA for RBD (HPLC)  
394 was purified by reversed phase chromatography. Messenger RNA was encapsulated into  
395 lipid nanoparticles (LNP) composed of ionizable lipid, phospholipid, cholesterol, and

396 PEG-lipid.

397

### 398 **Reagents**

399 Overlapping 20-aa peptides of spike protein were synthesized and purchased from  
400 Eurofins Genomics (Ebersberg, Germany). The SARS-CoV-2 spike protein (ECD) and  
401 RBD were purchased from GenScript (Piscataway, NJ, USA).

402

### 403 **Virus**

404 SARS-CoV-2 isolates were propagated in VeroE6 cells in Opti-MEM I (Invitrogen,  
405 Carlsbad, CA, USA) containing 0.3% bovine serum albumin (BSA) and 1  $\mu$ g of  
406 L-1-tosylamide-2-phenylethyl chloromethyl ketone (TPCK)-treated trypsin/mL at 37°C.

407

### 408 **Immunization**

409 Six to eight week-old C57BL/6 and BALB/c mice were intramuscularly immunized  
410 with mock, LNP-mRNA-RBD (3  $\mu$ g), or LNP-mRNA-RBD (HPLC) (3  $\mu$ g) on days 0  
411 and 14. Two weeks after the second immunization, the popliteal lymph nodes, spleen,  
412 and blood were collected. Cynomolgus macaques were intramuscularly immunized with  
413 mock or LNP-mRNA-RBD (HPLC) (100  $\mu$ g) on days 0 and 21. Blood was drawn on  
414 days 0, 7, 14, 21, and 28.

415

### 416 **ELISA**

417 ECD and RBD-specific antibody titers were measured using ELISA. In brief, half-area  
418 96-well plates were coated with ECD (1  $\mu$ g/mL) or RBD (1  $\mu$ g/mL) in bicarbonate  
419 buffer at 4°C. Plates were blocked with PBS containing 1% BSA for 60 min at room  
420 temperature. Plates were washed with PBST three times and incubated with diluted  
421 plasma or swab samples at room temperature for 120 min. Plates were washed with  
422 PBST three times and incubated with HRP-labeled goat anti-mouse IgG, IgG1, IgG2a,  
423 IgG2c, or mouse anti-monkey IgG at room temperature for 120 min. After washing with  
424 PBST three times, TMB substrate buffer was added, followed by incubation at room  
425 temperature for 10 min. Then, 1 N H<sub>2</sub>SO<sub>4</sub> was added to stop the reaction. OD values at  
426 450 and 540 or 560 nm were measured using a spectrophotometer. The reciprocal value  
427 of the plasma dilution with OD<sub>450</sub>–OD<sub>540</sub> or OD<sub>450</sub>–OD<sub>560</sub> of 0.2 was defined as the  
428 antibody titer.

429 Single-cell suspensions of splenocytes from immunized mice were stimulated by  
430 peptide pools 1–8, ECD, and RBD protein for 24 hours. IFN- $\gamma$  and IL-13 levels in the  
431 supernatant were measured using ELISA (R&D).

432

### 433 **GC B cell and T<sub>FH</sub> staining**

434 Single-cell suspensions of popliteal lymph nodes were stained with LIVE/DEAD Aqua,  
435 anti-CD279 (29F.1A12), San Diego, CA, USA), anti-CD8a (53-6.7), anti-CD3e  
436 (145-2C11), anti-GL7 (GL7), anti-CD4 (RM4-5), anti-CD185 (L138D7), anti-CD38  
437 (90), and anti-CD19 (6D5) antibodies. All antibodies were purchased from BioLegend,  
438 San Diego, CA, USA. The percentage of GC B cells and T<sub>FH</sub> cells was analyzed by flow  
439 cytometry.

440

### 441 **Intracellular staining assay for cytokines**

442 Single-cell suspensions of splenocytes were stimulated with peptide pools 2, 3, and 4  
443 together with protein transport inhibitors (eBioscience, San Diego, CA, USA) for 6 h.  
444 After stimulation, the cells were stained with LIVE/DEAD Aqua for dead cells. After  
445 washing, the cells were stained with anti-CD8a (53-6.7), anti-CD4 (RM4-5: Invitrogen),  
446 anti-TCR $\beta$  (H57-597), anti-F4/80 (RM8), anti-TER-119 (TER-119), anti-CD11b  
447 (M1/70), anti-CD19 (6D5), anti-CD11c (N418), anti-NK-1.1 (PK136), and  
448 anti-CD45R/B220 (RA3-6B2) antibodies. All antibodies were purchased from  
449 BioLegend unless otherwise stated. After fixation, permeabilization by IC Fixation  
450 Buffer (eBioscience), intracellular cytokines, and CD3 were stained with anti-IFN- $\gamma$   
451 (XMG1.2), anti-IL-2 (JES6-5H4), anti-TNF- $\alpha$  (MP6-XT22), and anti-CD3 (17A2)  
452 antibodies. All antibodies were purchased from BioLegend. The percentage of  
453 cytokine-producing CD8 $^{+}$  and CD4 $^{+}$  T cells was determined by flow cytometry.

454

### 455 **Preparation and stimulation of human peripheral blood mononuclear cells**

456 Peripheral blood mononuclear cells (PBMCs) were obtained from three  
457 SARS-CoV-2-uninfected healthy adult volunteers after obtaining informed consent. All  
458 experiments using human PBMCs were approved by the Institutional Review Board of  
459 the Institute of Medical Science, University of Tokyo. After preparation of PBMCs  
460 using Ficoll Histopaque, the cells were stimulated by LNP-mRNA-Full (0.4, 2, and 10  
461  $\mu$ g/mL), LNP-mRNA-RBD (0.4, 2, and 10  $\mu$ g/mL), or LNP-mRNA-RBD (HPLC) (0.4,

462 2, and 10 µg/mL) for 24 h. IFN- $\alpha$  level in the culture supernatant was measured using  
463 ELISA (Mabtech, Stockholm, Sweden).

464

#### 465 **Bone marrow-derived dendritic cells and stimulation**

466 Bone marrow-derived dendritic cells (BM-DCs) were differentiated by culturing for  
467 seven days with murine GM-CSF. Cells were stimulated with LNP-mRNA-Full (0.4, 2,  
468 and 10 µg/mL), LNP-mRNA-RBD (0.4, 2, and 10 µg/mL), or LNP-mRNA-RBD  
469 (HPLC) (0.4, 2, and 10 µg/mL) for 24 h. IFN- $\alpha$  in the culture supernatant was measured  
470 using ELISA (Invitrogen).

471

#### 472 **Neutralization activity against SARS-CoV-2 infection**

473 Thirty-five microliters of virus (140 tissue culture infectious dose 50) was incubated  
474 with 35 µL of two-fold serial dilutions of sera for 1 h at room temperature, and 50 µL of  
475 the mixture was added to confluent VeroE6/TMPRSS2 cells in 96-well plates and  
476 incubated for 1 h at 37°C. After the addition of 50 µL of DMEM containing 5% FCS,  
477 the cells were further incubated for three days at 37°C. Viral cytopathic effects (CPE)  
478 were observed under an inverted microscope, and virus neutralization titers were  
479 determined as the reciprocal of the highest serum dilution that completely prevented  
480 CPE <sup>24</sup>.

481

#### 482 **Virus titration using VeroE6/TMPRSS2 for SARS-CoV-2**

483 Confluent TMPRSS2-expressing Vero E6 cell line (JCRB Cell Bank, Japan) were  
484 incubated with diluted swab samples and 10% w/v tissue homogenate samples for 1 h.  
485 The cells were washed with HBSS and incubated with DMEM containing 0.1% BSA  
486 for three days <sup>25</sup>. Virus titers were monitored using a microscope and calculated using  
487 the Reed-Muench method.

488

#### 489 **Real-time RT-PCR for viral RNA**

490 Viral RNA from swab samples and tissues (20 mg) was collected using a QIAamp Viral  
491 RNA Mini kit and RNeasy Mini Kit, respectively. Viral RNA was measured by  
492 real-time RT-PCR (2019-nCoV\_N1-F, 2019-nCoV\_N1-R, 2019-nCoV\_N1-P, and  
493 TaqMan Fast Virus 1-step Master Mix) using CFX-96 (Bio-Rad, Hercules, CA, USA).

494

495 **Histological evaluation of lung section**

496 Lungs were obtained at autopsy, and 8 lung tissue slices were collected from each  
497 macaque: one slice from each upper lobe and middle lobe and two slices from each  
498 lower lobe in bilateral lungs. They were fixed in 10% neutral buffered formalin for  
499 approximately 72 h, embedded in paraffin and cut into 3- $\mu$ m-thick sections on glass  
500 slides. Sections were stained with hematoxylin and eosin (H & E) and observed under  
501 the light microscope. Histological evaluation was performed blindly by two pathologists  
502 based on a following criteria established in influenza virus infection <sup>26</sup> (0: normal lung,  
503 1: mild destruction of bronchial epithelium, 2: mild peribronchiolar inflammation, 3:  
504 inflammation in the alveolar walls resulting in alveolar thickening, 4: mild alveolar  
505 injury accompanied by vascular injury, 5: moderate alveolar injury and vascular injury,  
506 6, 7: severe alveolar injury with hyaline membrane-associated alveolar hemorrhage  
507 (under or over 50% of the section area)). The average score of 8 sections was calculated  
508 for each macaque, and the mean score of the two pathologists were defined as the  
509 histological score. SARS-CoV-2 N antigen was detected by a monoclonal antibody  
510 8G8A (Bioss Inc) and secondary antibody following antigen retrieval using autoclave in  
511 pH 9 citrate buffer.

512

513 **Body temperature**

514 Two weeks before virus inoculation, two temperature data loggers (iButton, Maxim  
515 Integrated, San Jose, CA) were implanted in the peritoneal cavity of each macaque  
516 under ketamine/xylazine anesthesia followed by isoflurane inhalation to monitor body  
517 temperature.

518

519 **X-ray radiography**

520 Chest X-ray radiographs were taken using the I-PACS system (Konica Minolta Inc.,  
521 Tokyo, Japan) and PX-20BT mini (Kenko Tokina Corporation, Tokyo, Japan).

522

523 **Statistical analysis**

524 Statistical significance ( $P < 0.05$ ) between groups was determined using the  
525 Mann-Whitney U test or ANOVA.

526

527 **Acknowledgments**

528 We thank Fusako Ikeda, Ryoko Suda, Yoko Watanabe, Naomi Sato, Naoko Kitagawa  
529 and Hideaki Ishida for technical assistance. This study was supported by AMED under  
530 Grant Number JP20fk0108113h0001 and JP20nk0101625h0201.

531

532 **Author contribution**

533 K.K., M.I., N.J., M.N., S.Y., Y.I., F.T., Y.K., K.J.I., designed research; K.K., M.I., N.J., M.N., K.H., K.I.H.,  
534 S.Yamayoshi., J.T., M.I., S.Yamada., T.W., M.K., H.N., H.I., Y.K., C.T.N., Y.I., performed research; K.K.,  
535 M.I., M.N., K.H., J.T., B.T., C.T.N., Y.I., analyzed data; N.J., T.N., T.S., F.T., contributed to provide  
536 LNP-mRNA vaccine. K.K., N.J., Y.I., Y.K., F.T., K.J.I. wrote the paper.

537

538 **Conflict of interest**

539 N.J., T.N., T.S., F.T., are employees of Daichi Sankyo Co., Ltd.  
540 K.K., M.I., N.J., S.Yamayoshi., T.N., T.S., F.T., Y.K., K.J.I. are inventors on patent  
541 application related to the content of this manuscript.

542

543 **References**

544

- 545 1 Baden, L. R. *et al.* Efficacy and Safety of the mRNA-1273 SARS-CoV-2  
546 Vaccine. *N Engl J Med*, doi:10.1056/NEJMoa2035389 (2020).
- 547 2 Polack, F. P. *et al.* Safety and Efficacy of the BNT162b2 mRNA  
548 Covid-19 Vaccine. *N Engl J Med* **383**, 2603-2615,  
549 doi:10.1056/NEJMoa2034577 (2020).
- 550 3 Lan, J. *et al.* Structure of the SARS-CoV-2 spike receptor-binding  
551 domain bound to the ACE2 receptor. *Nature* **581**, 215-220,  
552 doi:10.1038/s41586-020-2180-5 (2020).
- 553 4 Rydzynski Moderbacher, C. *et al.* Antigen-Specific Adaptive Immunity  
554 to SARS-CoV-2 in Acute COVID-19 and Associations with Age and  
555 Disease Severity. *Cell* **183**, 996-1012 e1019,  
556 doi:10.1016/j.cell.2020.09.038 (2020).
- 557 5 McMahan, K. *et al.* Correlates of protection against SARS-CoV-2 in  
558 rhesus macaques. *Nature*, doi:10.1038/s41586-020-03041-6 (2020).
- 559 6 Vogel, A. B. *et al.* BNT162b vaccines are immunogenic and protect  
560 non-human primates against SARS-CoV-2. *bioRxiv*,

561 2020.2012.2011.421008, doi:10.1101/2020.12.11.421008 (2020).

562 7 Zhou, P. *et al.* A pneumonia outbreak associated with a new  
563 coronavirus of probable bat origin. *Nature* **579**, 270-273,  
564 doi:10.1038/s41586-020-2012-7 (2020).

565 8 Jackson, L. A. *et al.* An mRNA Vaccine against SARS-CoV-2 -  
566 Preliminary Report. *N Engl J Med* **383**, 1920-1931,  
567 doi:10.1056/NEJMoa2022483 (2020).

568 9 Anderson, E. J. *et al.* Safety and Immunogenicity of SARS-CoV-2  
569 mRNA-1273 Vaccine in Older Adults. *N Engl J Med* **383**, 2427-2438,  
570 doi:10.1056/NEJMoa2028436 (2020).

571 10 Walsh, E. E. *et al.* Safety and Immunogenicity of Two RNA-Based  
572 Covid-19 Vaccine Candidates. *N Engl J Med* **383**, 2439-2450,  
573 doi:10.1056/NEJMoa2027906 (2020).

574 11 Elia, U. *et al.* Design of SARS-CoV-2 RBD mRNA Vaccine Using Novel  
575 Ionizable Lipids. *bioRxiv*, 2020.2010.2015.341537,  
576 doi:10.1101/2020.10.15.341537 (2020).

577 12 Tai, W. *et al.* A novel receptor-binding domain (RBD)-based mRNA  
578 vaccine against SARS-CoV-2. *Cell Res* **30**, 932-935,  
579 doi:10.1038/s41422-020-0387-5 (2020).

580 13 Lederer, K. *et al.* SARS-CoV-2 mRNA Vaccines Foster Potent  
581 Antigen-Specific Germinal Center Responses Associated with  
582 Neutralizing Antibody Generation. *Immunity* **53**, 1281-1295 e1285,  
583 doi:10.1016/j.jimmuni.2020.11.009 (2020).

584 14 Desmet, C. J. & Ishii, K. J. Nucleic acid sensing at the interface  
585 between innate and adaptive immunity in vaccination. *Nat Rev  
586 Immunol* **12**, 479-491, doi:10.1038/nri3247 (2012).

587 15 Coban, C. *et al.* Novel strategies to improve DNA vaccine  
588 immunogenicity. *Curr Gene Ther* **11**, 479-484,  
589 doi:10.2174/156652311798192815 (2011).

590 16 Pardi, N., Hogan, M. J., Porter, F. W. & Weissman, D. mRNA vaccines -  
591 a new era in vaccinology. *Nat Rev Drug Discov* **17**, 261-279,  
592 doi:10.1038/nrd.2017.243 (2018).

593 17 Iavarone, C., O'Hagan D, T., Yu, D., Delahaye, N. F. & Ulmer, J. B.

594 18 Mechanism of action of mRNA-based vaccines. *Expert Rev Vaccines* **16**,  
595 871-881, doi:10.1080/14760584.2017.1355245 (2017).

596 19 Kariko, K., Buckstein, M., Ni, H. & Weissman, D. Suppression of RNA  
597 recognition by Toll-like receptors: the impact of nucleoside  
598 modification and the evolutionary origin of RNA. *Immunity* **23**,  
599 165-175, doi:10.1016/j.jimmuni.2005.06.008 (2005).

600 20 Kariko, K. *et al.* Incorporation of pseudouridine into mRNA yields  
601 superior nonimmunogenic vector with increased translational  
602 capacity and biological stability. *Mol Ther* **16**, 1833-1840,  
603 doi:10.1038/mt.2008.200 (2008).

604 21 Kariko, K., Muramatsu, H., Ludwig, J. & Weissman, D. Generating  
605 the optimal mRNA for therapy: HPLC purification eliminates immune  
606 activation and improves translation of nucleoside-modified,  
607 protein-encoding mRNA. *Nucleic Acids Res* **39**, e142,  
608 doi:10.1093/nar/gkr695 (2011).

609 22 De Beuckelaer, A. *et al.* Type I Interferons Interfere with the Capacity  
610 of mRNA Lipoplex Vaccines to Elicit Cytolytic T Cell Responses. *Mol*  
611 *Ther* **24**, 2012-2020, doi:10.1038/mt.2016.161 (2016).

612 23 Linares-Fernandez, S., Lacroix, C., Exposito, J. Y. & Verrier, B.  
613 Tailoring mRNA Vaccine to Balance Innate/Adaptive Immune  
614 Response. *Trends Mol Med* **26**, 311-323,  
615 doi:10.1016/j.molmed.2019.10.002 (2020).

616 24 Corbett, K. S. *et al.* Evaluation of the mRNA-1273 Vaccine against  
617 SARS-CoV-2 in Nonhuman Primates. *N Engl J Med* **383**, 1544-1555,  
618 doi:10.1056/NEJMoa2024671 (2020).

619 25 Imai, M. *et al.* Syrian hamsters as a small animal model for  
620 SARS-CoV-2 infection and countermeasure development. *Proc Natl*  
621 *Acad Sci USA* **117**, 16587-16595, doi:10.1073/pnas.2009799117  
622 (2020).

623 26 Ishigaki, H. *et al.* Neutralizing antibody-dependent and -independent  
624 immune responses against SARS-CoV-2 in cynomolgus macaques.  
625 *Virology* **554**, 97-105, doi:10.1016/j.virol.2020.12.013 (2021).

626 26 Ogiwara, H. *et al.* Histopathological evaluation of the diversity of cells

627 susceptible to H5N1 virulent avian influenza virus. *Am J Pathol* **184**,  
628 171-183, doi:10.1016/j.ajpath.2013.10.004 (2014).  
629

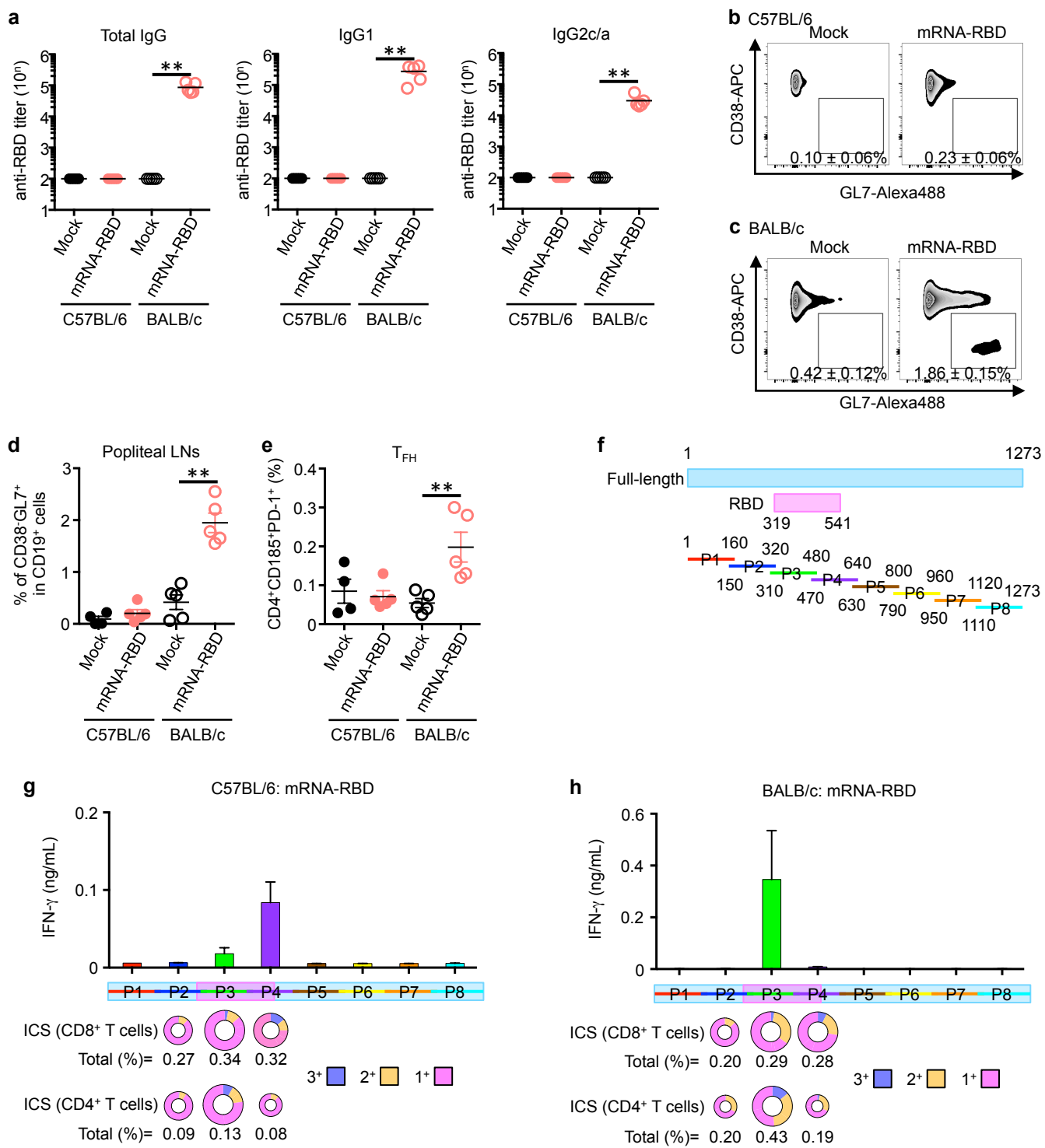


Figure. 1

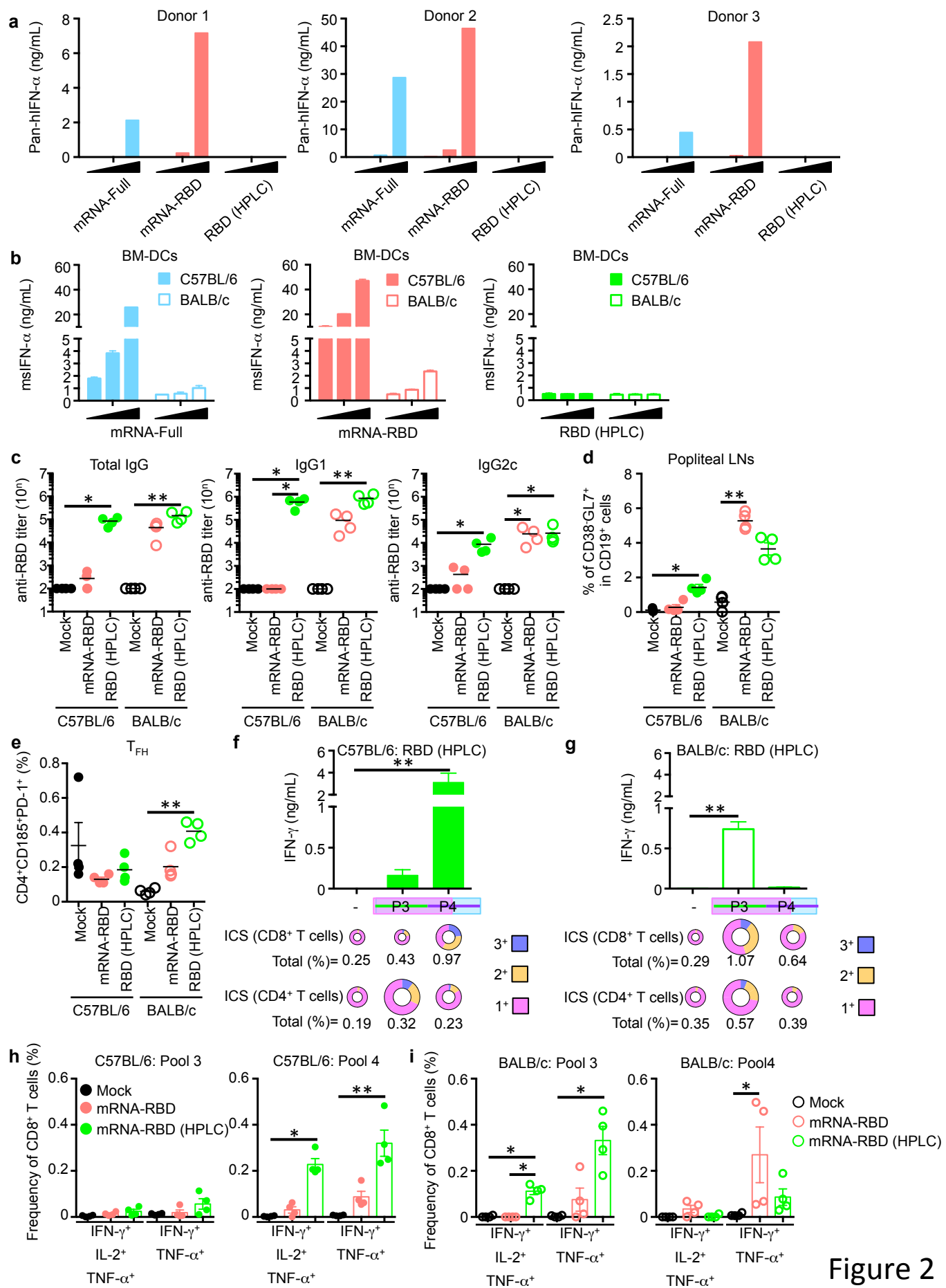
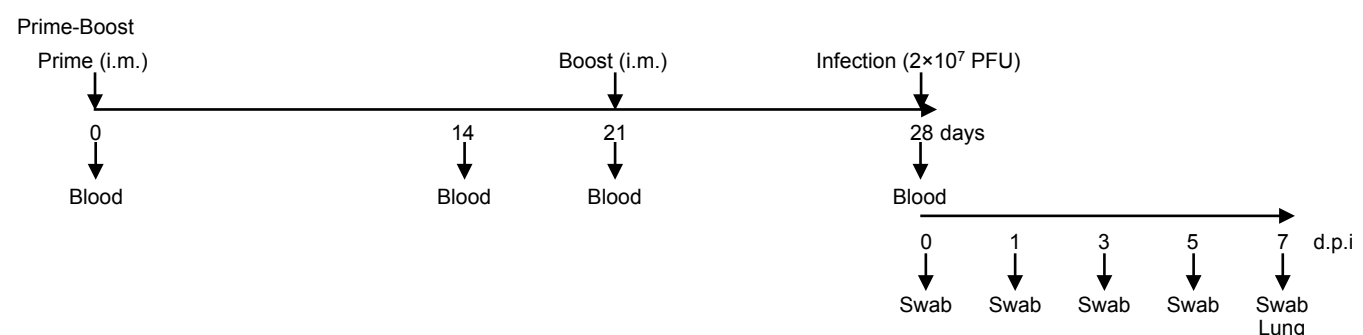
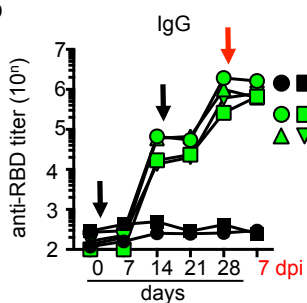


Figure 2

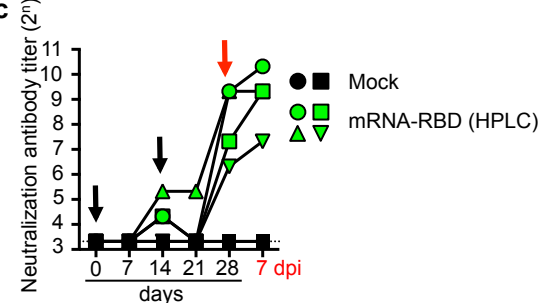
**a Cynomolgus Monkey**



**b**



**c**



**d**

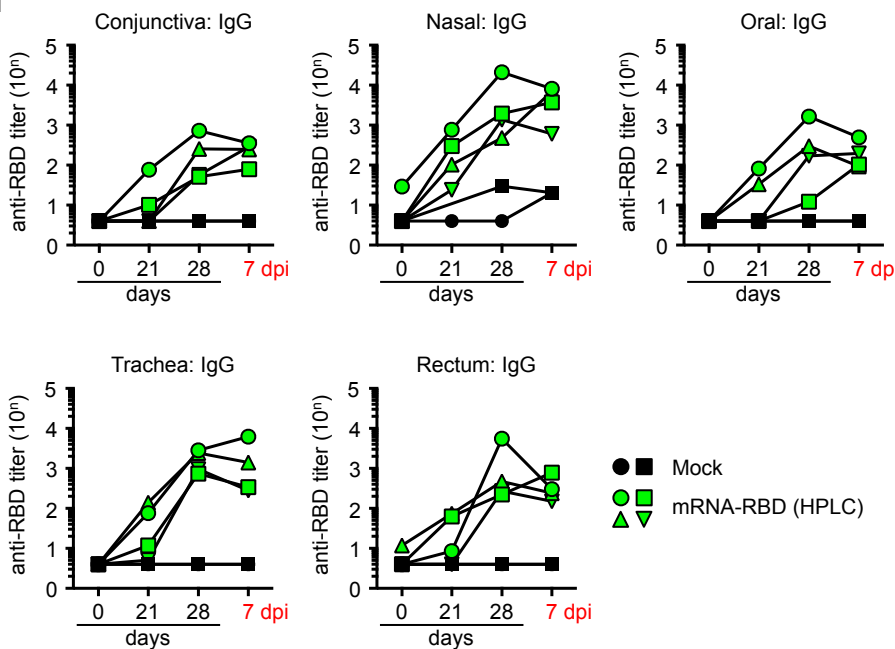


**Figure 3**

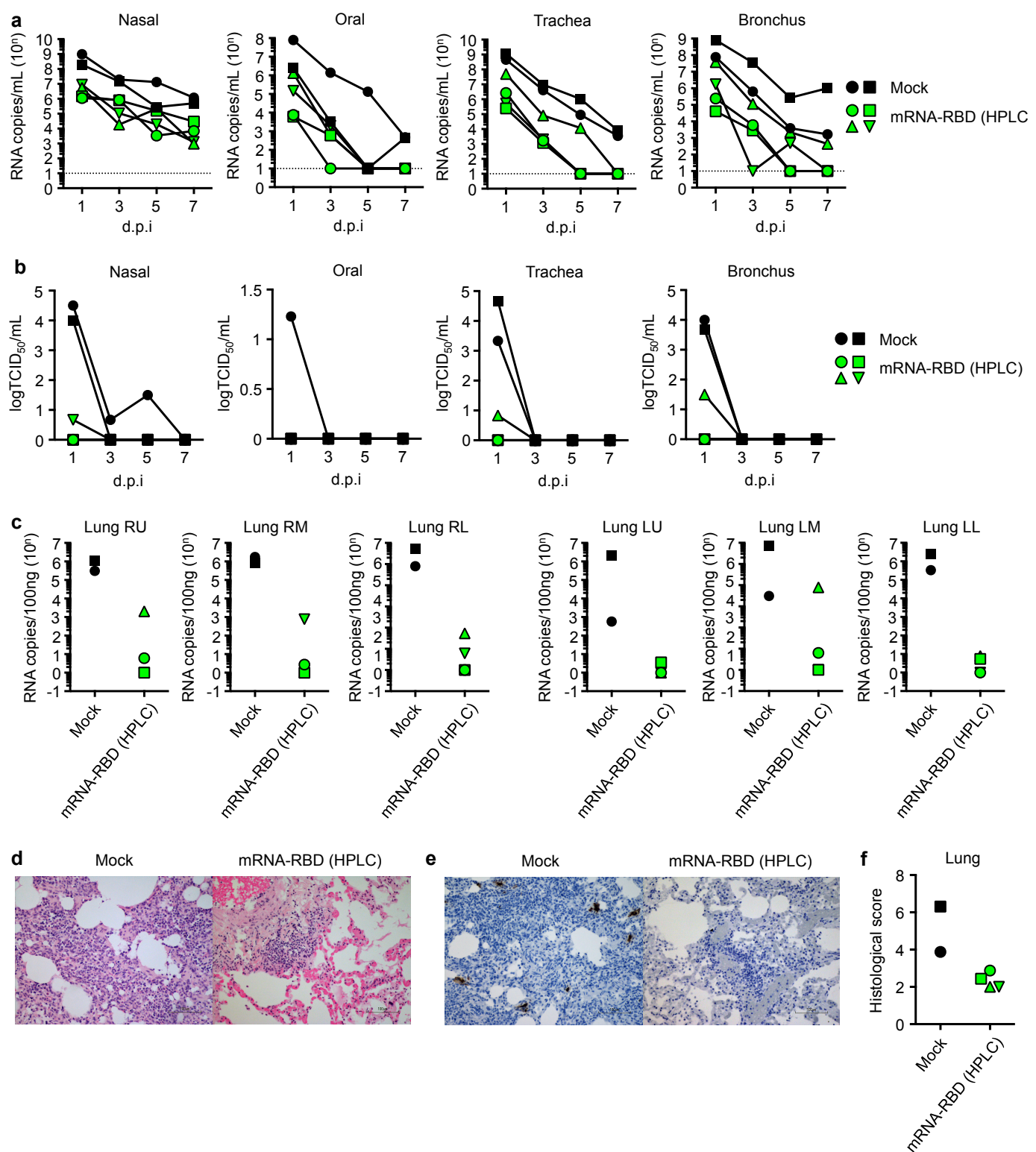
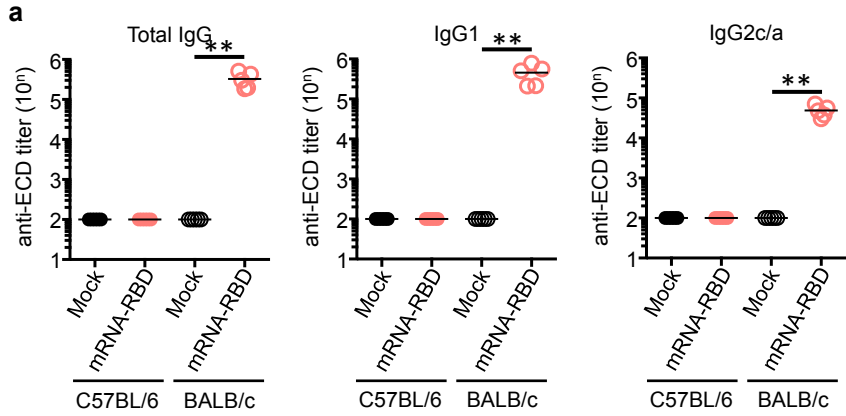
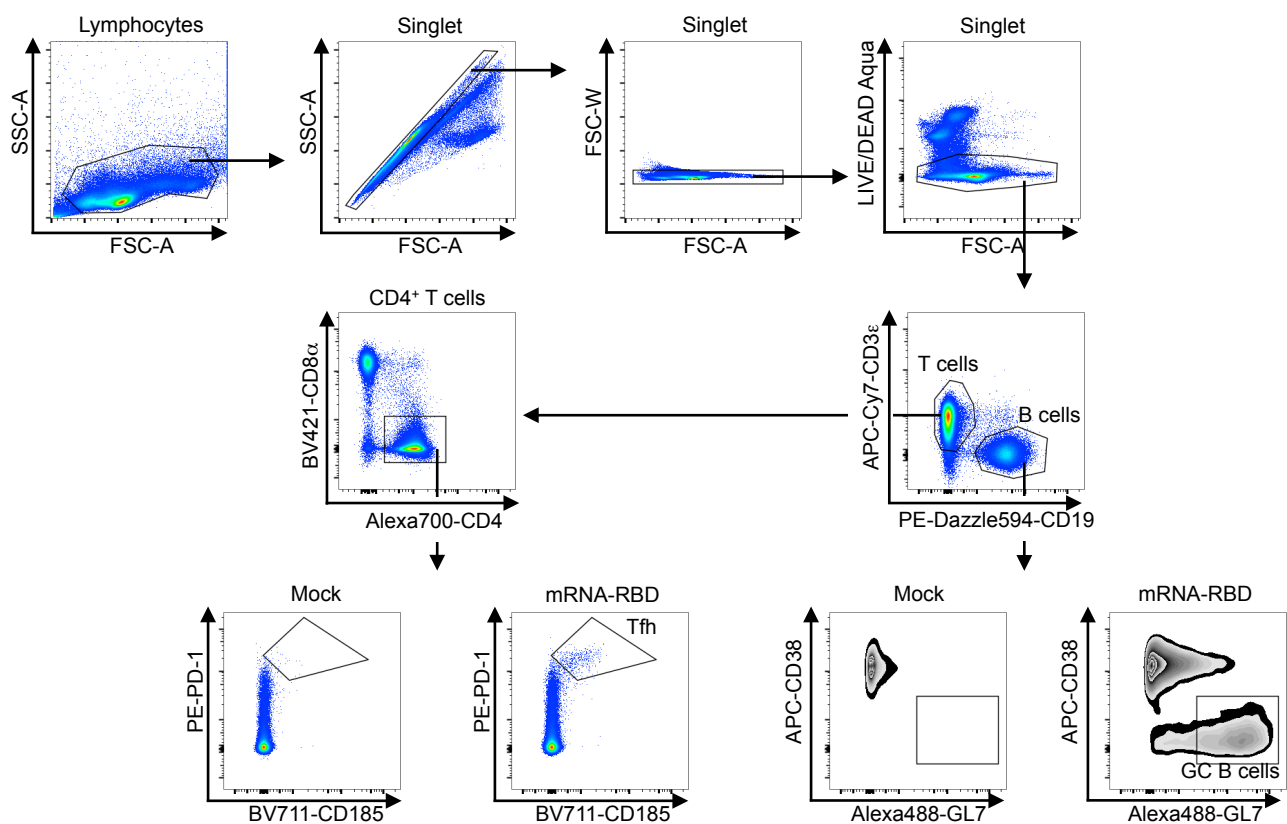


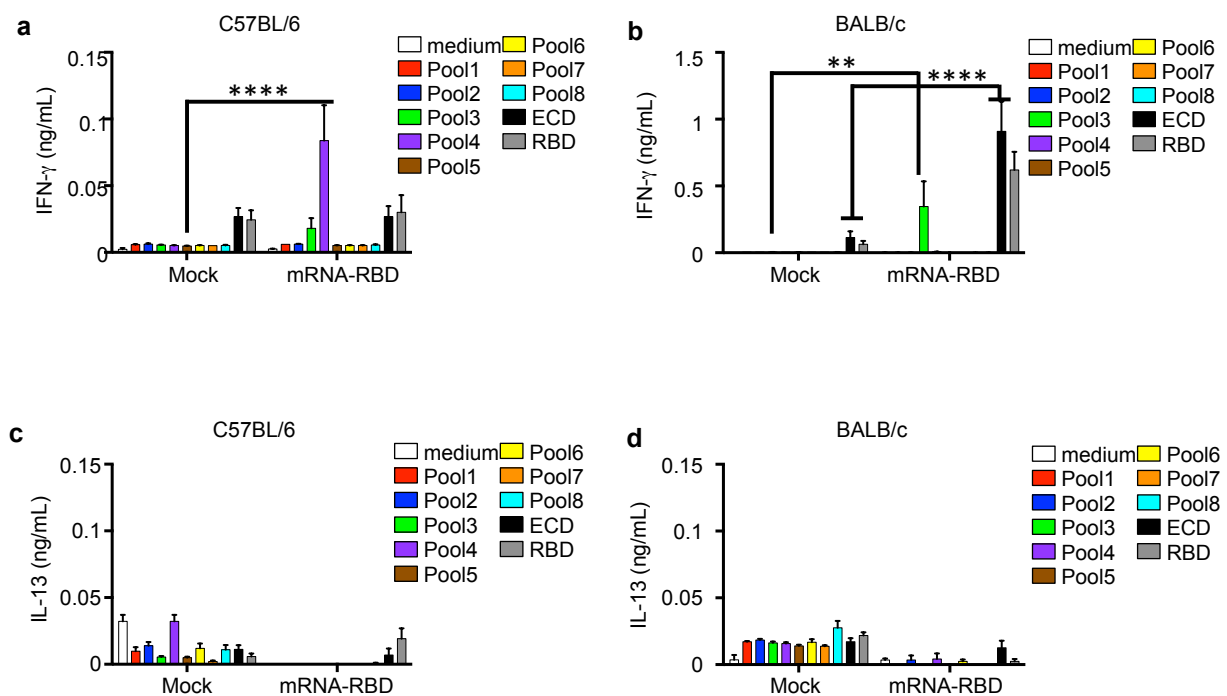
Figure 4



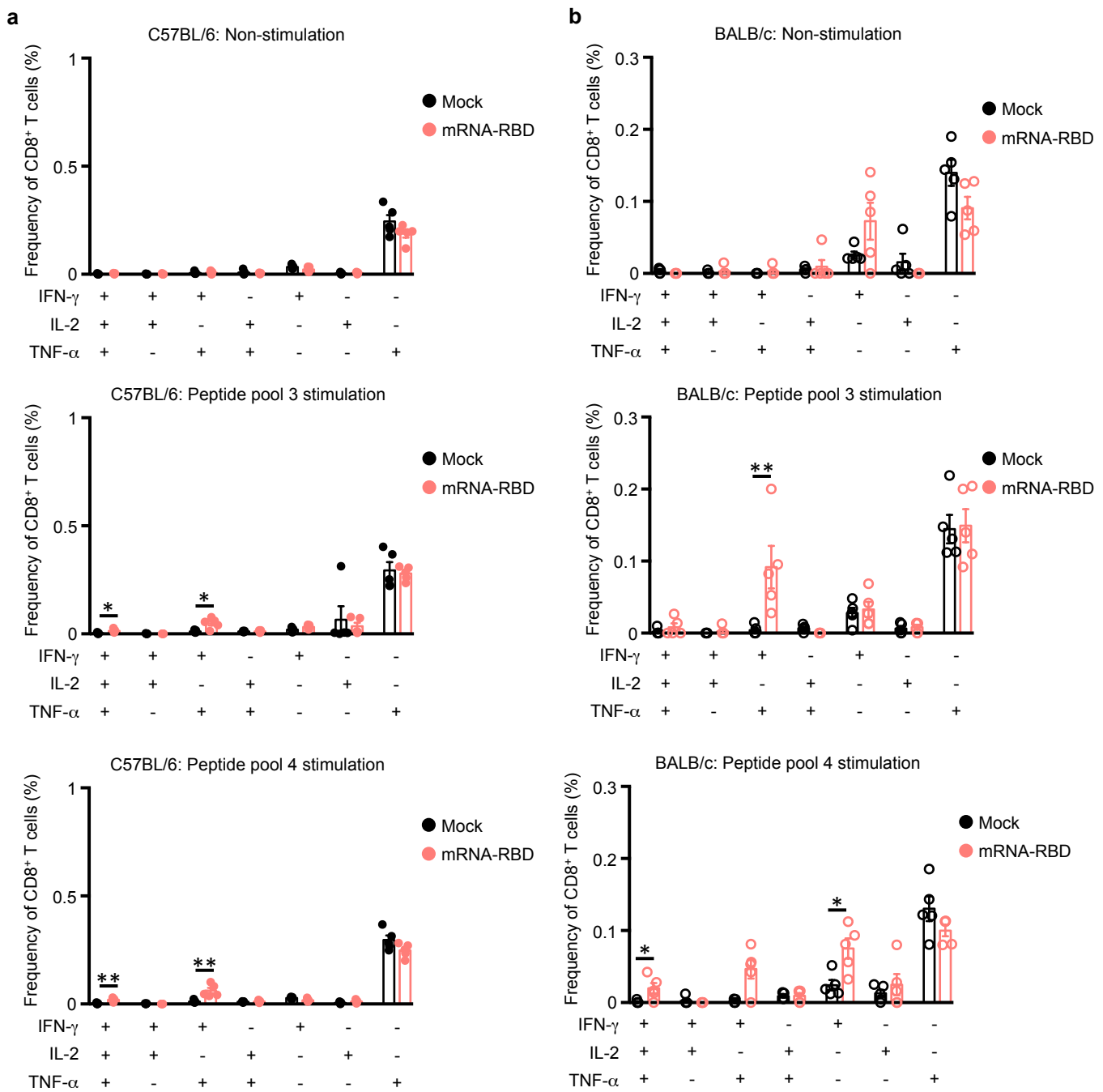
Extended data Fig. 1



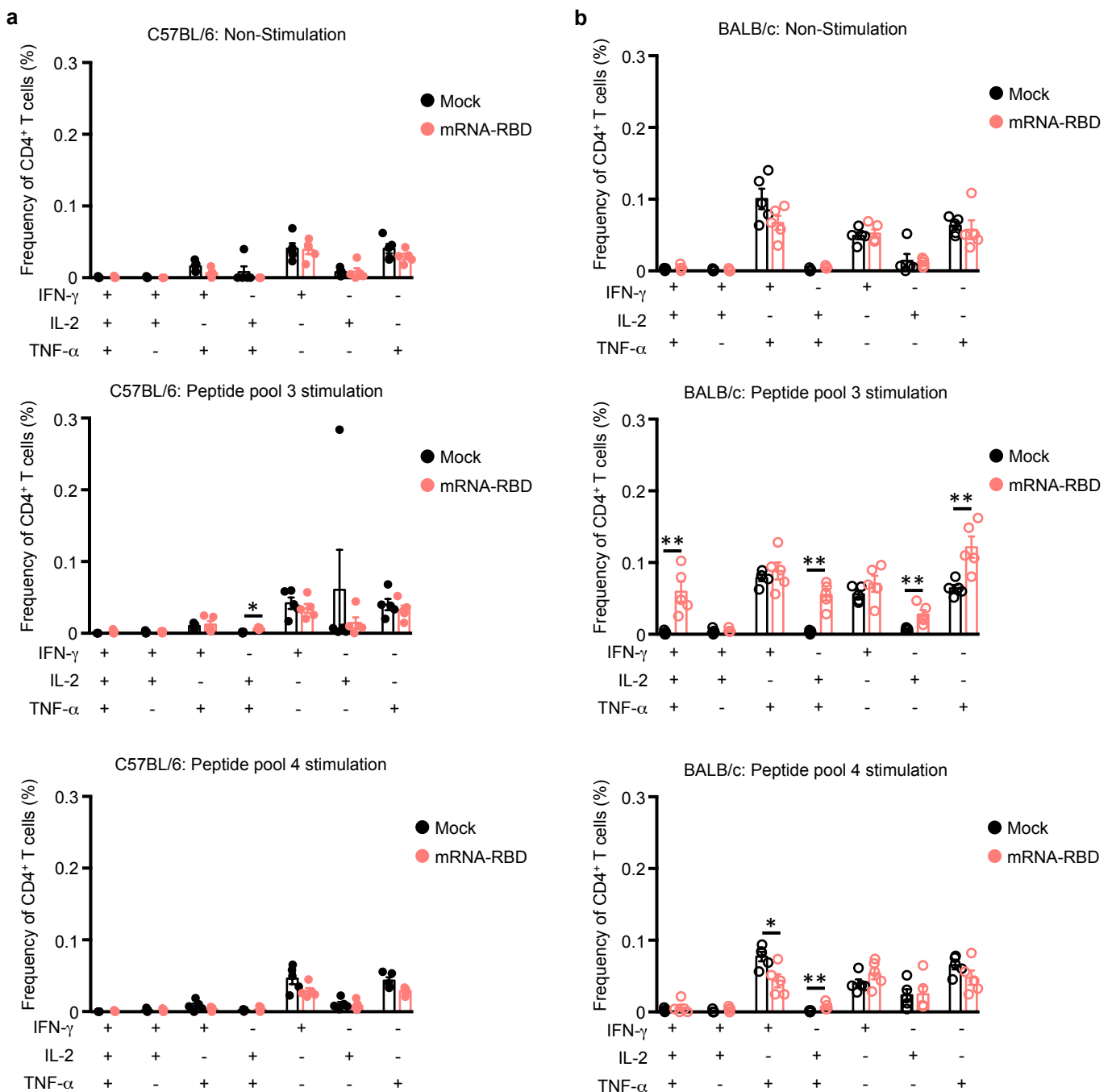
Extended data Fig. 2



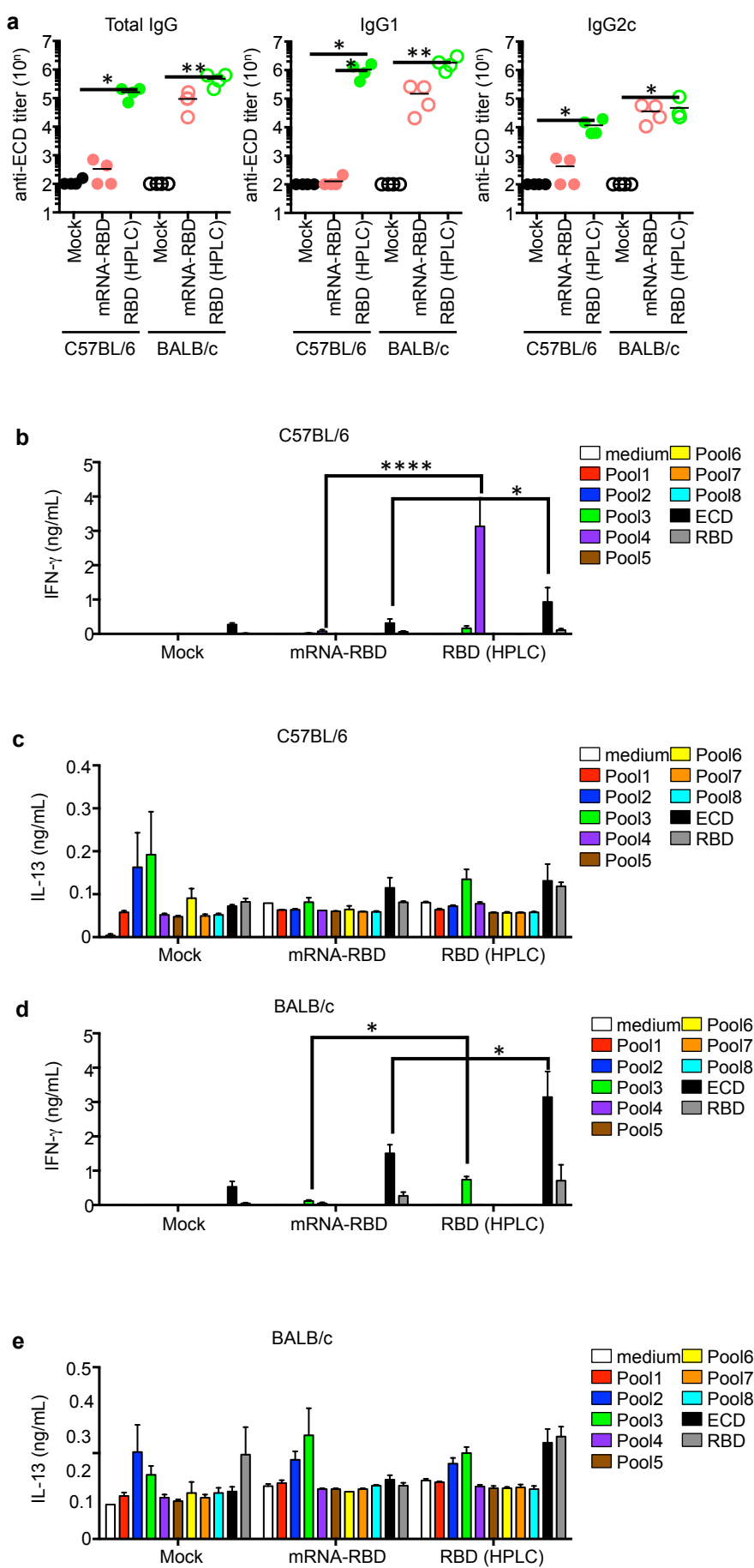
Extended data Fig. 3



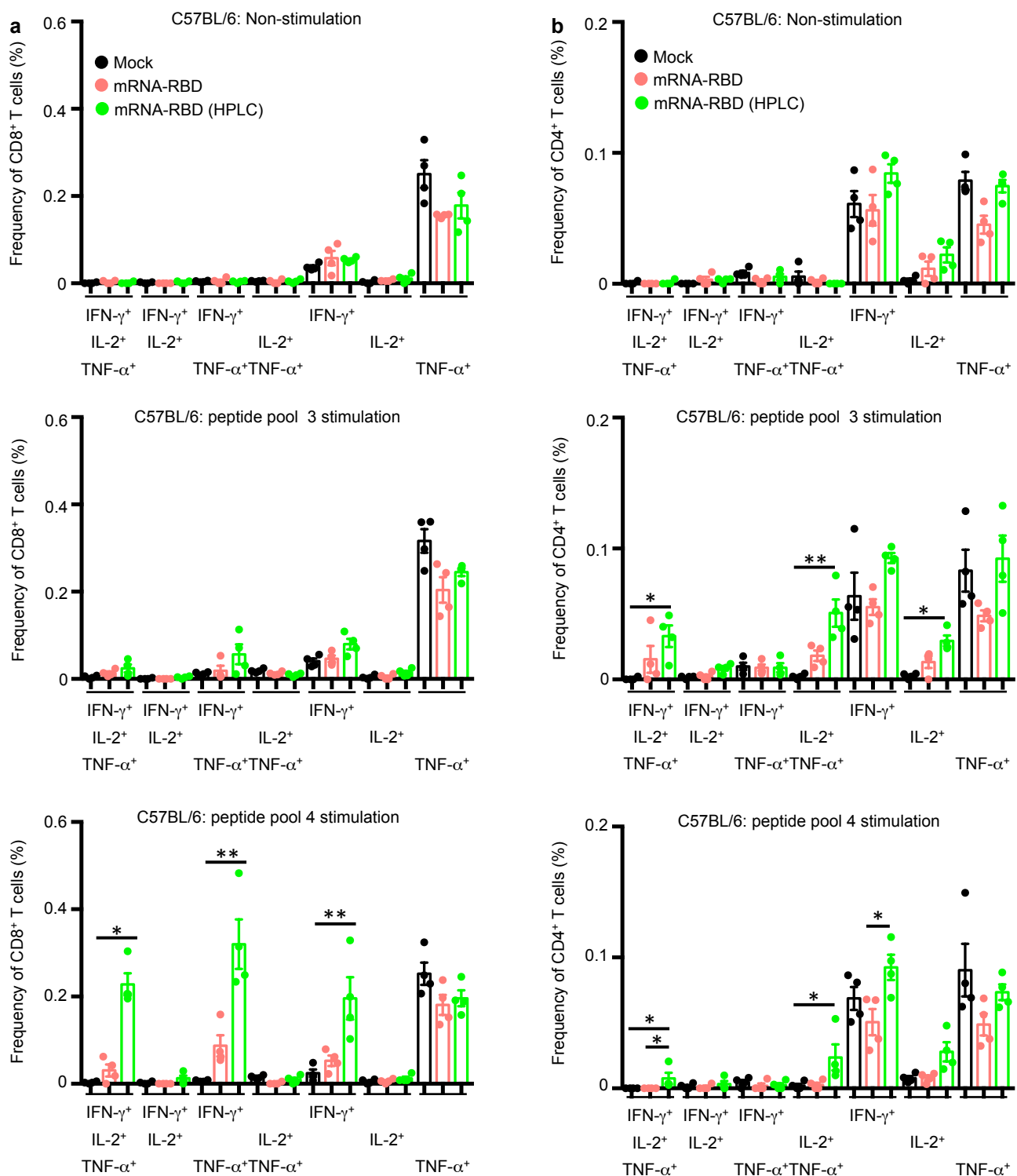
Extended data Fig. 4



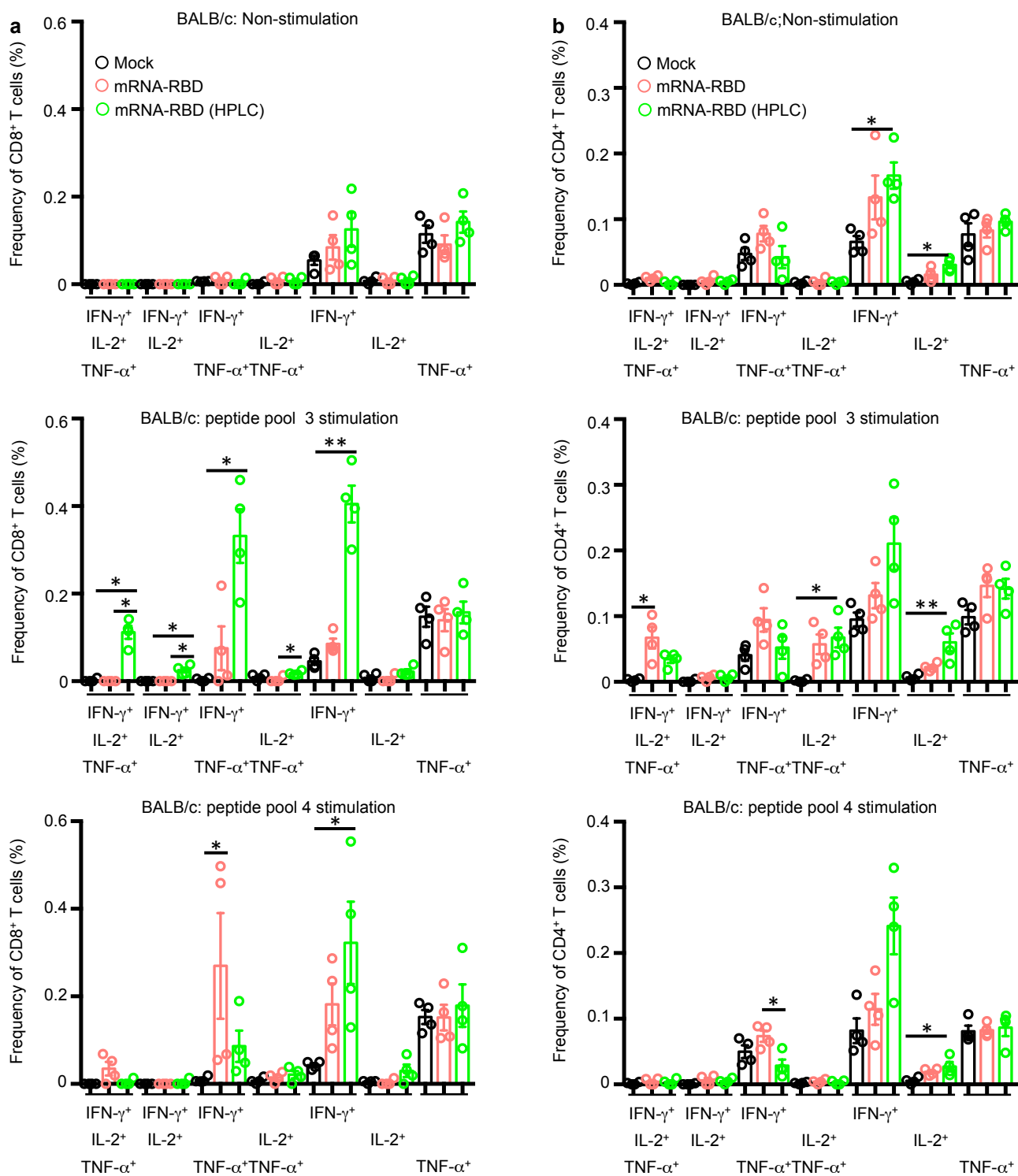
Extended data Fig. 5



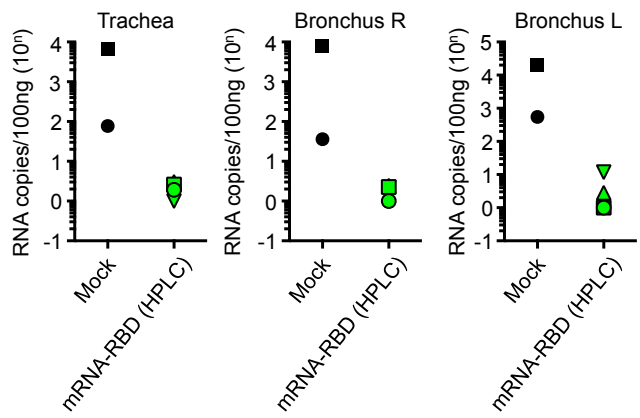
Extended data Fig. 6



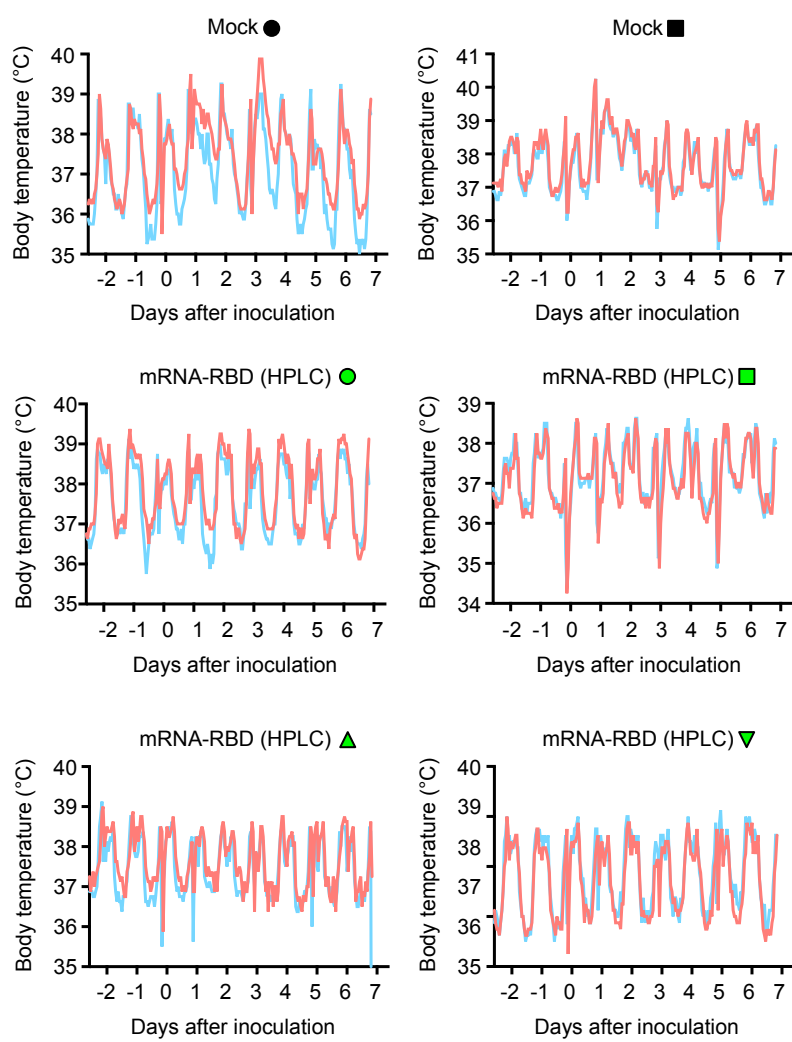
Extended data Fig. 7



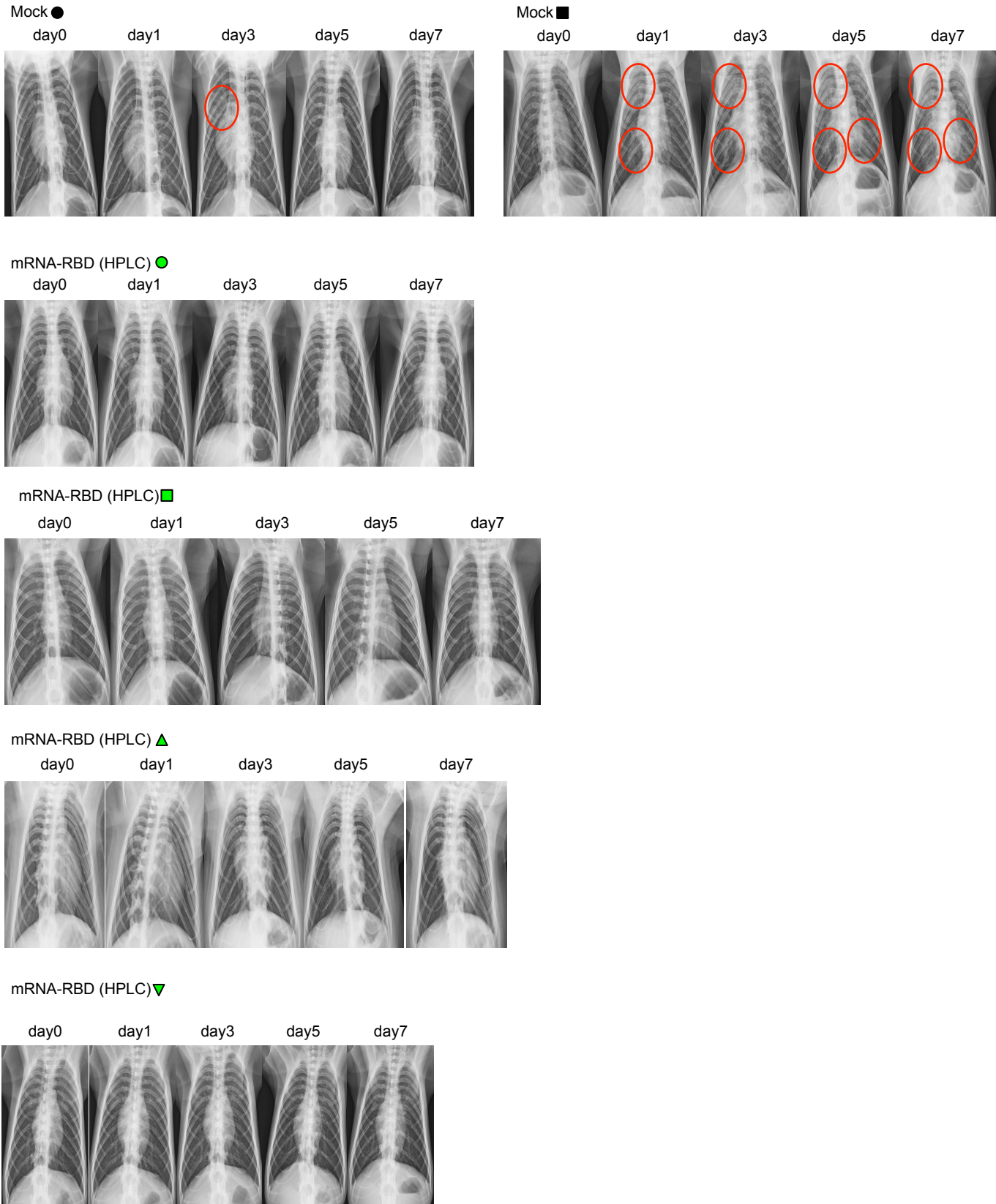
Extended data Fig. 8



Extended data Fig. 9



Extended data Fig. 10



Extended data Fig. 11